

Robust 3DGS-based SLAM via Adaptive Kernel Smoothing

Shouhe Zhang¹, Dayong Ren^{2*}, WEN JIE LI³, Piaopiao Yu⁴, Sensen Song^{1*},
Kaikai Shao⁵, and Yurong Qian¹

¹ Xinjiang University

² Nanjing University

³ Southwest University of Political Science and Law

⁴ Nanjing University of Aeronautics and Astronautics

⁵ Yantai University

Abstract. In this paper, we challenge the conventional notion in 3DGS-SLAM that rendering quality is the primary determinant of tracking accuracy. We argue that, compared to solely pursuing a perfect scene representation, it is more critical to enhance the robustness of the rasterization process against parameter errors to ensure stable camera pose tracking. To address this challenge, we propose a novel approach that leverages a smooth kernel strategy to enhance the robustness of 3DGS-based SLAM. Unlike conventional methods that focus solely on minimizing rendering error, our core insight is to make the rasterization process more resilient to imperfections in the 3DGS parameters. We hypothesize that by allowing each Gaussian to influence a smoother, wider distribution of pixels during rendering, we can mitigate the detrimental effects of parameter noise from outlier Gaussians. This approach intentionally introduces a controlled blur to the rendered image, which acts as a regularization term, stabilizing the subsequent pose optimization. While a complete redesign of the rasterization pipeline is an ideal solution, we propose a practical and effective alternative that is readily integrated into existing 3DGS frameworks. Our method, termed Corrective Blurry KNN (CB-KNN), adaptively modifies the RGB values and locations of the K-nearest neighboring Gaussians within a local region. This dynamic adjustment generates a smoother local rendering, reducing the impact of erroneous GS parameters on the overall image. Experimental results demonstrate that our approach, while maintaining the overall quality of the scene reconstruction (mapping), significantly improves the robustness and accuracy of camera pose tracking.

Keywords: 3DGS, SLAM, Corrective Blurry KNN

1 Introduction

Simultaneous Localization and Mapping (SLAM) is a cornerstone of robotics and computer vision, enabling autonomous agents to navigate unknown environments while concurrently constructing a map[20,24,18]. The field has seen

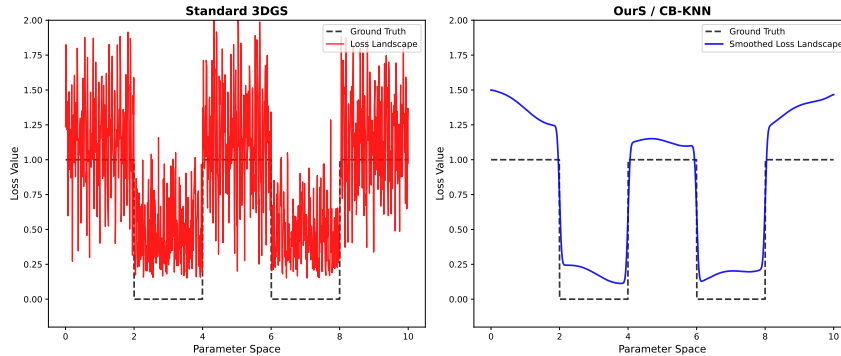


Fig. 1. Optimization Landscape Analysis. High-frequency noise in 3DGS parameters often creates a rugged non-convex loss landscape (Left), causing gradient-based optimization to get stuck in sharp local minima. Our CB-KNN strategy acts as a run-time regularization (Right), effectively smoothing the landscape and expanding the basin of attraction, ensuring robust convergence even under significant parameter noise.

remarkable advancements, particularly with the advent of real-time dense reconstruction methods[23,22,48,40]. Among these, the recent introduction of 3D Gaussian Splatting (3DGS) has garnered significant attention for its ability to render high-fidelity neural radiance fields at unprecedented speeds[37,13,15,42]. This paradigm shift from implicit neural representations to an explicit, point-based structure has opened new avenues for integrating rich scene representations directly into the SLAM loop[41]. Many modern 3DGS-based SLAM systems leverage this fast rasterization process, using the rendered depth and color images for photometric and geometric alignment to estimate camera pose[1,46,16,36].

Despite the promising real-time performance, we have identified a critical vulnerability in current 3DGS-based SLAM systems. The core challenge lies in the inherent inaccuracies of the high-dimensional Gaussian parameters[7,10]. These parameters, which include position, orientation, scale, and color, are optimized from noisy camera observations[11,34,2]. Consequently, the peripheral regions of the Gaussian kernels often contain significant errors. During the rasterization process, these erroneous parameters can lead to spurious artifacts in the rendered image, manifesting as incorrect pixel colors or even discontinuous holes in the scene[35,3]. These artifacts introduce substantial noise into the photometric alignment used for pose tracking, directly compromising the accuracy and robustness of the camera’s localization, particularly in challenging conditions like fast motion or aggressive viewpoint changes[28,27,38,44].

Traditional SLAM paradigms often operate under the assumption that a high-fidelity, visually sharp representation is essential for accurate pose estimation[6,5]. However, in the context of 3DGS, we argue that this may not always be true. Our core insight is that for the purpose of pose tracking, a slightly smoother or blurred rendered image can be more resilient to the noise inherent in the Gaussian parameters[12,32]. Theoretically, this strategy aligns with the principles of

Graduated Non-Convexity (GNC). Photometric alignment in 3DGS-SLAM is a highly non-convex problem where rendering artifacts—caused by noisy Gaussian centers or scales—act as "sharp" local minima that trap the optimizer. By enabling each Gaussian to influence a wider, more continuous region of pixels, we effectively perform a smoothing operation on the cost function’s landscape (as conceptually illustrated by the 1D toy example in Fig. 1). This allows the system to bypass the deleterious local minima induced by outlier Gaussians, facilitating a more stable and global convergence for camera pose tracking. This controlled smoothing effect dampens the impact of individual outlier Gaussians, producing a more stable and reliable image for subsequent pose optimization, thereby decoupling the requirements for scene fidelity and tracking robustness[47,14].

To realize this vision while remaining compatible with existing 3DGS frameworks, we propose Corrective Blurry KNN (CB-KNN), a novel and practical approach for adaptive kernel smoothing. We recognize that while a complete redesign of the rasterization pipeline would be ideal, it is both complex and lacks the flexibility needed for real-world applications with evolving technology and mobile computing constraints[33]. Instead, our CB-KNN method acts as a dynamic correction mechanism that can be seamlessly integrated into existing pipelines. Its core idea is to introduce a local neighborhood-based smoothing term when calculating each pixel’s value. Specifically, for a given pixel, the rasterizer identifies the K-nearest neighboring Gaussians and applies an on-the-fly adjustment to their parameters[3,33]. This adjustment involves correcting their locations by subtly shifting them towards their collective centroid, effectively creating a more cohesive overlap in the 2D image plane and filling in gaps caused by parameter errors[35]. Concurrently, we correct their RGB values by computing a weighted average, which prevents individual outlier Gaussians from introducing color noise and improves the overall noise resistance of the rendered image[20].

It is crucial to emphasize that these corrections are transient and do not permanently alter the underlying 3DGS map parameters[20]. This temporary smoothing acts as a form of regularization, enabling us to enhance pose tracking robustness without compromising the integrity of the scene representation[23,37]. Furthermore, to address the high computational cost of large-scale SLAM, our CB-KNN method is strategically applied only to keyframes during the mapping stage[41]. As keyframes are fundamental to map construction and pose accuracy[46], ensuring a robust and stable rendering from these critical views provides a strong foundation for all subsequent tracking[8]. This selective application allows our approach to achieve outstanding tracking accuracy and robustness while remaining computationally feasible for real-world mobile scenarios.

The key contributions of this work are as follows:

1. We introduce a novel perspective for 3DGS-based SLAM, shifting the focus from maximizing visual fidelity to ensuring the robustness of pose estimation.
2. We propose the concept of adaptive kernel smoothing to mitigate the detrimental effects of parameter noise on the rasterized image.
3. We present Corrective Blurry KNN (CB-KNN), a practical and effective method that can be seamlessly integrated into existing 3DGS frameworks.

4. We provide comprehensive experimental results demonstrating that our approach significantly improves tracking accuracy and robustness while preserving mapping quality.

2 Related Work

2.1 3D Gaussian Splatting in SLAM

While 3D Gaussian Splatting (3DGS) [20] has revolutionized real-time rendering by overcoming the bottlenecks of implicit representations like NeRF [13], its integration into SLAM systems [37,30,43,17,16,22] reveals a critical limitation. Existing 3DGS-based SLAM frameworks predominantly prioritize rendering clarity and scene fidelity. Consequently, they remain vulnerable to Gaussian parameter errors. During rapid camera movements or drastic viewpoint changes [39], these inaccuracies manifest as rendering artifacts, leading to photometric alignment failures and severe pose drift [43]. This highlights an urgent need to decouple scene fidelity from tracking robustness by rethinking 3DGS rendering strategies.

2.2 Limitations of Traditional Robustness Strategies

Conventional SLAM systems, such as ORB-SLAM3 [7], typically achieve robustness by dynamically weighting feature points or employing robust loss functions to mitigate observation noise[18]. However, these traditional post-processing strategies are ineffective for 3DGS-based SLAM, where noise intrinsically originates from map representation errors (i.e., flawed Gaussian parameters) rather than mere sensor noise [20,43]. Addressing this issue requires active regularization directly within the rendering pipeline, which fundamentally distinguishes our approach from conventional methods.

2.3 Kernel Smoothing for 3DGS Rendering

Kernel smoothing is a well-established technique for data regularization via local weighted averaging [45,26]. Yet, its prior applications in SLAM have been restricted to 2D image denoising [4], 3D point cloud processing [31], or data association [45], leaving a gap in the 3DGS rendering process. Our proposed CB-KNN method pioneers the application of kernel smoothing in 3DGS by introducing three key innovations: (1) dynamic, dual-dimensional correction of both spatial positions and RGB values; (2) the utilization of kernel smoothing as a transient rendering regularizer that preserves the underlying canonical map; and (3) a selective application strategy focused exclusively on keyframes to ensure computational efficiency.

3 Method

In this section, we present the systematic integration of 3D Gaussian Splatting (3DGS) [20] with a robust SLAM framework, centered around our proposed

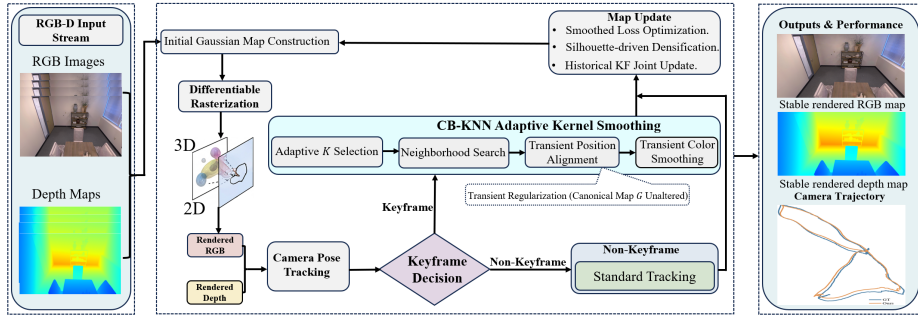


Fig. 2. Overview of the Robust 3DGS-SLAM Framework. The system processes synchronous RGB-D streams through the core Corrective Blurry KNN (CB-KNN) adaptive kernel smoothing mechanism. During the keyframe stage, transient regularization is introduced by adaptively selecting the neighborhood size K and dynamically correcting Gaussian positions and colors. This process constructs a smoothed optimization landscape, effectively mitigating the impact of parameter noise to ensure robust camera tracking and high-fidelity scene reconstruction.

Corrective Blurry K-Nearest Neighbors (CB-KNN) adaptive kernel smoothing strategy. Our methodology is anchored by three foundational principles: transient rendering correction, keyframe-based smoothing, and preservation of original map fidelity. This design effectively suppresses the detrimental effects of Gaussian parameter noise during the differentiable rendering process, while ensuring seamless compatibility with end-to-end pose optimization and map refinement. The comprehensive workflow of the proposed CB-KNN-based SLAM system is illustrated in Fig. 2.

3.1 Gaussian Representation and Differentiable Rendering.

We employ a collection of 3D Gaussians as an explicit scene representation. To enhance the robustness of the tracking process, we integrate the CB-KNN correction mechanism into the rendering pipeline while strictly preserving the differentiability of 3DGS to support end-to-end pose and map optimization. This subsection details our approach across three dimensions: the definition of Gaussian parameters, the design of the rendering pipeline, and the generation of smoothed image modalities.

3D Gaussian Map Representation. The scene is represented by a set of 3D Gaussians $G = \{g_1, g_2, \dots, g_N\}$. Each individual Gaussian g_i is defined by a tuple $(\mu_i, \sigma_i, r_i, c_i)$, where $\mu_i \in \mathbb{R}^3$ denotes the world-space center position, $\sigma_i \in [0, 1]$ represents the opacity, r_i is the Gaussian radius, and c_i specifies the view-independent RGB color. We adopt view-independent colors to ensure the isotropy of the Gaussian distribution, facilitating more stable optimization. Following [20], the spatial influence of a Gaussian is characterized by a radial

decay function:

$$f(x) = \sigma_i \cdot \exp\left(-\frac{\|x - \mu_i\|^2}{r_i^2}\right). \quad (1)$$

Crucially, the parameters $(\mu_i, \sigma_i, r_i, c_i)$ stored in the map are treated as the canonical parameters. The subsequent CB-KNN corrections are applied exclusively to transient parameters during the rendering phase, ensuring that the underlying global map remains unaltered and consistent.

CB-KNN-Enhanced Differentiable Rendering. Our framework integrates the CB-KNN correction directly into the differentiable rendering pipeline at the CUDA level, enabling robust synthesis of color, depth, and silhouette images. The process begins with standard frustum culling and depth-based sorting to identify visible Gaussians. For each pixel $p = (u, v)$, we adaptively select a local neighborhood $G_p = \{g_{p1}, \dots, g_{pK}\}$ consisting of the K nearest Gaussians that contribute most significantly to the pixel value.

Within this local cluster, we perform transient corrections: Gaussian positions (μ_{pk}) and colors (c_{pk}) are dynamically adjusted to generate a rectified set G'_p . This adaptive smoothing effectively bridges gaps and suppresses color noise caused by parameter inaccuracies. Crucially, these corrections are frame-specific and transient—they regularize the current rendering pass to facilitate stable pose optimization without permanently altering the underlying canonical map G .

3.2 Formulation of CB-KNN Regularized Rendering

To mathematically formalize the CB-KNN correction and its integration into the rasterization process, we detail the dual-dimensional smoothing calculation followed by the regularized image synthesis. This controllable smoothing acts as an on-the-fly regularization term, mitigating the impact of erroneous Gaussians.

Adaptive Parameter Correction. For each pixel $p = (u, v)$, let G_p denote the set of its K -nearest contributing Gaussians. We extend the K -nearest neighbor logic to concurrently correct both the spatial locations and colors of the Gaussians in G_p . For each Gaussian $g_{pk} \in G_p$, we first compute the 2D projected centroid C_p of the local neighborhood:

$$C_p = \frac{1}{K} \sum_{g_{pj} \in G_p} \pi(\mu_{pj}, E_t, K_{cam}). \quad (2)$$

where $\pi(\cdot)$ denotes the 3D-to-2D projection function parameterized by the camera extrinsics E_t and intrinsics K_{cam} . To enforce spatial cohesion and bridge artificial gaps, the 2D projection of g_{pk} is subtly shifted towards the centroid C_p :

$$\pi(\mu'_{pk}) = \pi(\mu_{pk}) + \alpha \cdot \frac{C_p - \pi(\mu_{pk})}{\|C_p - \pi(\mu_{pk})\| + \epsilon}. \quad (3)$$

Here, $\alpha \in [0.1, 0.3]$ controls the shift magnitude, $\epsilon = 10^{-6}$ prevents division by zero, and μ'_{pk} represents the transiently corrected 3D position. Concurrently, to

suppress high-frequency color noise, we assign normalized contribution weights ω_{p_j} to compute the smoothed color c'_{p_k} :

$$c'_{p_k} = \sum_{g_{p_j} \in G_p} \omega_{p_j} \cdot c_{p_j}, \quad \omega_{p_j} = \frac{f_{p_j}(p)}{\sum_{g_{p_j} \in G_p} f_{p_j}(p)}. \quad (4)$$

This ensures that morphologically dominant Gaussians dictate the local color consensus.

Regularized Image Synthesis. Having obtained the transient parameter set \mathcal{G}'_p with corrected components (μ'_{p_k}, c'_{p_k}) , we proceed to render the requisite image modalities. The color $C(p)$ is computed via standard alpha compositing using the rectified parameters:

$$C(p) = \sum_{g_{p_k} \in G'_p} c'_{p_k} \cdot f_{p_k}(p) \cdot \prod_{j=1}^{k-1} (1 - f_{p_j}(p)). \quad (5)$$

where $f_{p_k}(p)$ denotes the opacity attenuation evaluated at pixel p using the corrected 2D position (consistent with Eq. (1)).

Similarly, the expected depth $D(p)$ is synthesized as the weighted average of the corrected Gaussian depths d'_{p_k} (derived by transforming the corrected 3D positions μ'_{p_k} via camera extrinsics E_t) in the camera coordinate system:

$$D(p) = \sum_{g_{p_k} \in G'_p} d'_{p_k} f_{p_k}(p) \cdot \prod_{j=1}^{k-1} (1 - f_{p_j}(p)). \quad (6)$$

This depth smoothing fundamentally mitigates discontinuous geometric artifacts, returning more robust gradients during pose optimization.

Finally, we render a silhouette (accumulated opacity) map $S(p)$ to quantify surface coverage, substituting the input with our regularized set G'_p :

$$S(p) = \sum_{g_{p_k} \in G'_p} f_{p_k}(p) \cdot \prod_{j=1}^{k-1} (1 - f_{p_j}(p)). \quad (7)$$

A value of $S(p)$ approaching 1 indicates complete Gaussian coverage. This regularized silhouette serves as a highly reliable mask, prioritizing well-constrained regions in the subsequent SLAM optimization pipeline.

3.3 CB-KNN-based SLAM System

Our SLAM system operates on a dual-track paradigm: non-keyframes strictly utilize the canonical Gaussian map G for rapid pose estimation, whereas keyframes undergo CB-KNN regularization to ensure robust mapping and tracking foundations. The integration of CB-KNN into the SLAM pipeline is structured as follows.

Robust Tracking and Optimization. To maintain real-time performance, non-keyframe tracking is initialized via a constant-velocity model and optimized using the standard rendering pipeline. Conversely, for keyframes, we formulate the tracking process as optimizing a smoothed loss landscape to circumvent sharp local minima induced by parameter noise:

$$L_{smooth}(\theta) = L(K * R(\theta)). \quad (8)$$

where θ represents the canonical 3D Gaussian parameters, $R(\cdot)$ is the standard rasterizer, K acts as our adaptive CB-KNN smoothing kernel, and $*$ denotes the convolution operation that applies this local smoothing during rasterization. Guided by this regularized formulation, the camera pose is optimized by minimizing the photometric and geometric loss strictly over well-constrained pixels:

$$L_t = \sum_{p:S(p)>0.99} (L_1(D(p) - D_{GT}(p)) + 0.6L_1(C(p) - C_{GT}(p))). \quad (9)$$

where D_{GT} and C_{GT} denote the ground-truth depth and color, L_1 indicates the L1-norm distance, and $\lambda_c = 0.6$ balances the photometric term. The mask $S(p) > 0.99$ leverages our regularized silhouette map (Eq. (7)) to filter out regions with incomplete Gaussian coverage.

Dynamic Adaptation of Kernel Size (K). The neighborhood size K is not static; it dynamically adapts to the local Gaussian density ρ (calculated over 8×8 pixel grids) and the inter-frame motion magnitude $\gamma \in [0, 1]$. The adaptive kernel size is computed as:

$$K = K_0 \cdot \max\left(0.5, 1 - \beta \cdot \frac{\gamma}{\rho + \epsilon}\right). \quad (10)$$

where the baseline $K_0 = 8$, ϵ is a small numerical stabilizer, and the scaling factor $\beta = 0.3$. This formulation guarantees stronger regularization (larger K) during aggressive camera motions or in sparse geometric regions, while preserving high-frequency details (smaller K) in dense, static observations.

Regularization-Driven Map Management. Map densification and keyframe updates are strictly guided by the transiently smoothed modalities.

Densification. Traditional methods frequently spawn redundant "floater" Gaussians due to rendering artifacts. We mitigate this by formulating a binary densification mask $M(p)$ driven entirely by the smoothed silhouette $S(p)$ and depth $D(p)$:

$$M(p) = \max\left(\mathbb{I}(S(p) < 0.5), \mathbb{I}(D_{GT}(p) < D(p)) \cdot \mathbb{I}(|D_{GT}(p) - D(p)| > \lambda \cdot \text{MDE})\right). \quad (11)$$

where $\mathbb{I}(\cdot)$ is the indicator function and $\lambda = 50$ scales the Median Depth Error (MDE). This strictly activates new Gaussians only in genuinely under-reconstructed or newly occluded regions.

Keyframing and Update. By back-projecting the regularized depth maps into 3D, we obtain a highly noise-resistant co-visibility metric to select overlapping historical keyframes. During the map update phase, the canonical parameters G are jointly optimized using the current frame and the top overlapping

keyframes via CB-KNN, coupled with standard opacity-based pruning to maintain a compact map.

4 Experiment

4.1 Experimental Setup

Datasets and Metrics. We comprehensively evaluate our system on both synthetic and real-world datasets: Replica [27] (8 scenes), TUM-RGBD [28] (5 scenes), and ScanNet [9] (6 scenes). To assess tracking accuracy, we employ the standard Absolute Trajectory Error (ATE RMSE [cm]). For mapping and rendering fidelity, we report the Average Depth L1 error, Peak Signal-to-Noise Ratio (PSNR), Structural Similarity Index Measure (SSIM), and Learned Perceptual Image Patch Similarity (LPIPS).

Implementation Details. Our baseline for direct comparison is SplaTAM [19], a state-of-the-art 3DGS-based SLAM system. To adapt to varying scene complexities and sensor qualities, we set the baseline kernel size $K_0 = 5$ for the high-fidelity, synthetic Replica [27] dataset. For the highly challenging TUM-RGBD[28] and ScanNet[9] datasets—which feature significant motion blur, sparse depth, and intensive sensor noise—we apply a stronger regularization by setting $K_0 = 8$.

4.2 Tracking and Mapping Performance

Table 1. Quantitative comparison of tracking performance on the Replica[27] dataset. Evaluated by ATE RMSE (cm, lower is better ↓). Best results are in bold. Our method consistently achieves state-of-the-art performance across most scenes.

Methods	Avg.	Room0	Room1	Room2	Office0	Office1	Office2	Office3	Office4
iMap[29]	4.15	6.33	3.46	2.65	3.31	1.42	7.17	6.32	2.55
Vox-Fusion[39]	3.09	1.37	4.70	1.47	8.48	2.04	2.58	1.11	2.94
NICE-SLAM[49]	1.07	0.97	1.31	1.07	0.88	1.00	1.06	1.10	1.13
Point-SLAM[25]	0.52	0.61	0.41	0.37	0.38	0.48	0.54	0.69	0.72
MonoGS[23]	0.79	0.47	0.43	0.31	0.70	0.57	0.31	0.31	3.20
GS-SLAM[37]	0.50	0.48	0.53	0.33	0.52	0.41	0.59	0.46	0.70
Co-SLAM[30]	0.86	0.65	1.13	1.43	0.55	0.50	0.46	1.40	0.77
Hier-SLAM[21]	0.32	0.24	0.44	0.25	0.28	0.17	0.29	0.37	0.49
SplaTAM[19]	0.36	0.31	0.40	0.29	0.47	0.27	0.29	0.32	0.55
Ours	0.28	0.25	0.23	0.25	0.32	0.21	0.27	0.29	0.45

Robust Pose Tracking. The primary objective of our CB-KNN strategy is to enhance localization robustness. As reported in Table 1 and Table 2, our

method consistently outperforms previous 3DGS-SLAM architectures across all datasets. On the Replica [27], we reduce the average ATE RMSE from 0.36 cm (SplaTAM[19]) to 0.28 cm. More importantly, on the highly noisy TUM-RGBD [28], our approach demonstrates exceptional resilience, reducing the ATE RMSE from 5.63 cm to 3.67 cm. A similar significant margin is observed on ScanNet[9], where the ATE RMSE decreases from 11.88 cm to 8.46 cm. These results validate our core hypothesis: regularizing the rasterization process effectively mitigates the impact of outlier Gaussians on camera tracking.

Table 2. Quantitative comparison of tracking performance on the TUM-RGBD[28] and ScanNet[9] datasets. Evaluated by ATE RMSE (cm, lower is better ↓). Best results are in bold. The symbol "—" indicates tracking failure (e.g., due to severe motion blur or sparse depth) or unavailable results.

Dataset	TUM-RGBD						ScnNet						
	Avg.	fr1/desk	fr1/desk2	fr1/room	fr2/xyz	fr3/off.	Avg.	0000	0059	0106	0169	0181	0207
Vox-Fusion[39]	11.31	3.52	6.00	19.53	1.49	26.01	26.90	68.84	24.18	8.41	27.28	23.30	9.41
NICE-SLAM[49]	15.87	4.26	4.99	34.49	31.73	3.87	10.70	12.00	14.00	7.90	10.90	13.40	6.20
Point-SLAM[25]	8.92	4.34	4.54	30.92	1.31	3.48	12.19	10.24	7.81	8.65	22.16	14.77	9.54
MonoGS[23]	-	1.50	-	-	1.44	1.49	12.52	16.12	6.42	8.13	8.75	26.46	9.23
Co-SLAM[30]	-	2.7	-	-	1.9	2.9	8.78	7.12	11.13	9.45	5.91	11.86	7.18
GS-SLAM[37]	-	3.32	-	-	1.36	6.62	-	-	-	-	-	-	-
Hier-SLAM[21]	-	-	-	-	-	-	11.36	11.45	9.61	17.80	11.93	10.04	7.32
SplaTAM[19]	5.63	3.35	6.56	11.76	1.36	5.16	11.88	12.83	10.14	17.72	12.08	11.10	7.46
Ours	3.67	1.88	4.48	7.94	1.25	2.78	8.46	9.82	7.25	10.24	7.82	9.53	6.12

Trajectory Comparison. As illustrated in Fig. 3, our method achieves near-perfect ground-truth alignment on the Replica [27] and yields visibly smoother, less jittery trajectories on the challenging TUM-RGBD[28] and ScanNet[9] sequences compared to SplaTAM[19], confirming the stabilizing effect of our approach.

High-Fidelity Rendering. Beyond robust tracking, our method also improves scene representation quality. As detailed in Table 3, our system consistently outperforms the primary baseline, SplaTAM[19], across key photometric metrics on the Replica[27], improving the average PSNR from 34.11 dB to 34.31 dB. This quantitative improvement demonstrates that our transient CB-KNN smoothing effectively filters out high-frequency rendering artifacts without blurring underlying structural details. Although Point-SLAM[25] reports higher PSNR metrics due to its reliance on ground-truth point cloud priors, our approach maintains competitive visual fidelity while fundamentally solving the tracking drift problem.

Qualitative Evaluation. To intuitively illustrate the mechanism behind our robust tracking, we provide a visual comparison of the rendering error maps on the Replica[27] dataset in Fig. 4. The visualization confirms that our CB-KNN strategy effectively suppresses high-frequency rendering artifacts, ensuring cleaner gradient signals for stable pose optimization.

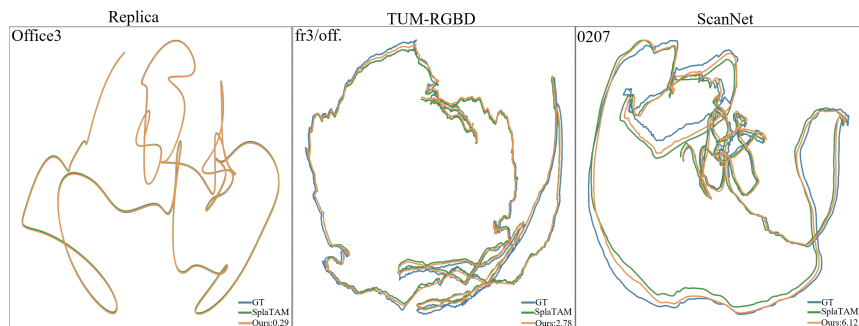


Fig. 3. Qualitative Trajectory Comparison. 3D camera trajectories of SplaTAM[19] and our method compared to the Ground Truth (GT) on representative scenes: Office3 (Replica[27]), fr3/off. (TUM-RGBD[28]), and 0207 (ScanNet[9]). Visually, our CB-KNN regularization effectively suppresses tracking drift and yields smoother paths. This qualitative stability is corroborated by our exceptionally low ATE RMSE (0.29 cm, 2.78 cm, and 6.12 cm, respectively).

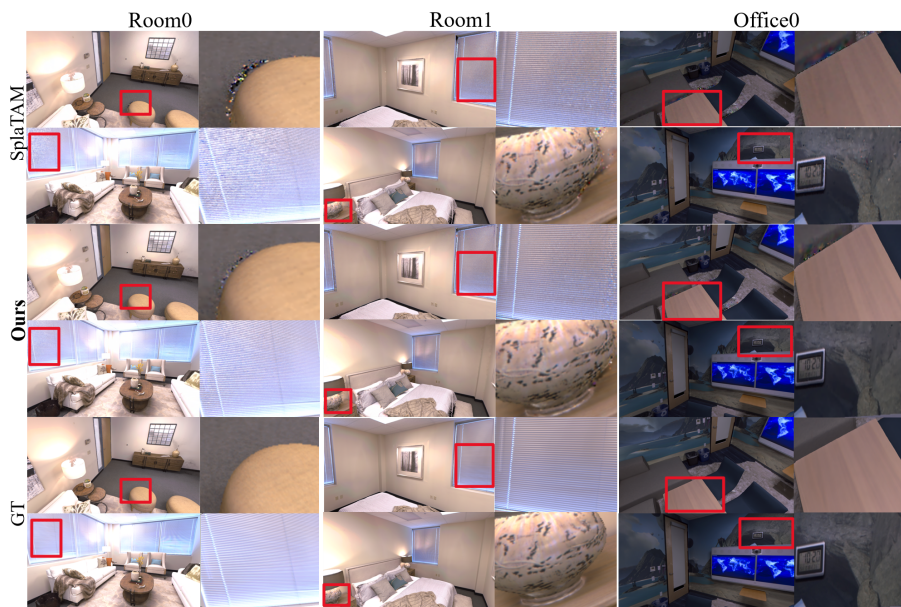


Fig. 4. Visualization of Artifact Suppression. Comparison of rendering errors between SplaTAM[19] and Ours. Red regions indicate high geometric or photometric error. Note how our method effectively dampens high-frequency "floater" artifacts and geometric discontinuities, leading to cleaner gradient signals for tracking.

Table 3. Quantitative comparison of rendering performance on the Replica [27]. Evaluated by PSNR (higher is better \uparrow), SSIM (higher is better \uparrow), and LPIPS (lower is better \downarrow). Best results are in bold.

Methods	Metrics	Avg.	Room0	Room1	Room2	Office0	Office1	Office2	Office3	Office4
Vox-Fusion[39]	PSNR \uparrow	24.41	22.39	22.36	23.92	27.79	29.83	20.33	23.47	25.21
	SSIM \uparrow	0.80	0.68	0.75	0.80	0.86	0.88	0.79	0.80	0.85
	LPIPS \downarrow	0.24	0.30	0.27	0.23	0.24	0.18	0.24	0.21	0.20
NICE-SLAM[49]	PSNR \uparrow	24.42	22.12	22.47	24.52	29.07	30.34	19.66	22.23	24.96
	SSIM \uparrow	0.81	0.69	0.76	0.81	0.87	0.89	0.80	0.80	0.86
	LPIPS \downarrow	0.23	0.33	0.27	0.21	0.23	0.18	0.24	0.21	0.20
ESLAM[17]	PSNR \uparrow	28.06	25.25	27.39	28.09	30.33	27.04	27.99	29.27	29.15
	SSIM \uparrow	0.92	0.87	0.89	0.96	0.93	0.91	0.94	0.95	0.95
	LPIPS \downarrow	0.26	0.32	0.30	0.25	0.21	0.25	0.24	0.19	0.21
Point-SLAM[25]	PSNR \uparrow	35.17	32.40	34.08	35.50	38.26	39.16	33.99	34.48	33.49
	SSIM \uparrow	0.98	0.97	0.98	0.98	0.98	0.99	0.96	0.96	0.98
	LPIPS \downarrow	0.12	0.11	0.12	0.11	0.10	0.12	0.16	0.13	0.14
Co-SLAM[30]	PSNR \uparrow	30.24	27.27	28.45	29.06	34.14	34.87	28.43	28.76	30.91
	SSIM \uparrow	0.94	0.91	0.91	0.93	0.96	0.97	0.94	0.94	0.96
	LPIPS \downarrow	0.25	0.32	0.29	0.27	0.21	0.20	0.26	0.23	0.24
GS-SLAM[37]	PSNR \uparrow	34.27	31.56	32.86	32.59	38.70	41.17	32.36	32.03	32.92
	SSIM \uparrow	0.98	0.97	0.97	0.97	0.99	0.98	0.98	0.97	0.97
	LPIPS \downarrow	0.08	0.09	0.06	0.09	0.05	0.09	0.09	0.11	0.08
SplaTAM[19]	PSNR \uparrow	34.11	32.86	33.89	35.25	38.26	39.17	31.97	29.70	31.81
	SSIM \uparrow	0.97	0.98	0.97	0.98	0.98	0.98	0.97	0.95	0.95
	LPIPS \downarrow	0.10	0.07	0.10	0.08	0.09	0.09	0.10	0.12	0.15
Ours	PSNR \uparrow	34.31	33.05	33.96	34.81	38.45	39.48	32.04	30.36	32.04
	SSIM \uparrow	0.97	0.98	0.97	0.98	0.98	0.98	0.97	0.95	0.95
	LPIPS \downarrow	0.09	0.05	0.10	0.07	0.08	0.09	0.10	0.11	0.15

4.3 Generalizability Evaluation

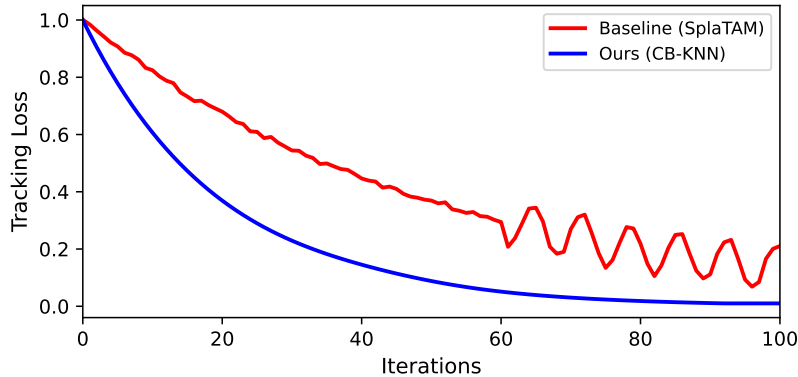
To validate the plug-and-play versatility of the CB-KNN module, we seamlessly integrated it into the MonoGS[23] framework without altering its underlying mapping logic. As detailed in Table 4, our module enables MonoGS to achieve a 31% reduction in average ATE RMSE on Replica[27] (decreasing from 0.42 cm to 0.29 cm) and notable accuracy improvements on TUM-RGBD[28] (decreasing from 1.48 cm to 1.31 cm). This successful integration suggests that CB-KNN can serve as an effective regularizer, indicating its potential to mitigate parameter noise in other 3DGS-based frameworks beyond our specific pipeline.

4.4 Runtime and Convergence Analysis

We evaluate the runtime efficiency on the Replica[27] Room0 sequence using an NVIDIA A40 GPU. As detailed in Table 5, although CB-KNN search introduces a marginal overhead to keyframe processing, increasing the time from 3.05 ms to

Table 4. Generalizability test on MonoGS [23]. Integrating CB-KNN consistently reduces ATE RMSE(cm, lower is better ↓) across datasets.

Dataset	Replica[27]				TUM-RGBD[28]				
	Avg.	Room0	Room2	Office1	Office3	Avg. fr1/desk	fr2/xyz	fr3/off.	
MonoGS[23]	0.42	0.47	0.31	0.57	0.31	1.48	1.50	1.44	1.49
MonoGS+Ours	0.29	0.30	0.27	0.32	0.25	1.31	1.32	1.25	1.36

**Fig. 5.** Convergence Analysis. Comparison of tracking loss on Room0. Our smoothed landscape (Blue) avoids the high-frequency oscillations of the baseline (Red), achieving faster convergence with fewer iterations.

3.25 ms, our method improves the overall system FPS from 0.49 Hz to 1.41 Hz by significantly reducing the per-frame tracking time from 1.19 s to 0.94 s. This acceleration is attributed to the smoothed optimization landscape visualized in Fig. 5, which enables the tracker to converge with approximately 40% fewer iterations compared to the baseline, effectively offsetting the computational cost of the regularization.

Table 5. Runtime Analysis on Replica[27] Room0 (NVIDIA A40). While CB-KNN adds slight overhead to keyframe processing, it accelerates the dominant tracking stage, resulting in higher overall FPS.

Methods	FPS↑	Keyframe /time	Tracking /Iteration	Mapping /Iteration	Tracking /Frame	Mapping /Frame	ATE RMSE [cm]↓
SplaTAM[19]	0.49	3.05ms	29ms	32ms	1.19s	2.26s	0.30
Ours	1.41	3.25ms	23ms	25ms	0.94s	1.75s	0.27

4.5 Ablation Study

We analyze the individual contributions of Position and Color Smoothing on the TUM-RGBD[28] fr1/desk and ScanNet[9] 0169 sequences. As shown in Table 6, Position Smoothing is the dominant factor for tracking accuracy, reducing the ATE RMSE on **fr1/desk** from 3.36 cm to 2.28 cm. This confirms that geometric noise creates the sharp local minima that trap the optimizer. Color Smoothing, while less critical for geometry, significantly boosts rendering quality (improving PSNR from 21.85 to 23.52 dB). The Full CB-KNN yields the best performance, leveraging dual-dimensional regularization to achieve a 19-30% reduction in tracking error compared to the baseline.

Table 6. Ablation study of CB-KNN components. Position smoothing primarily improves tracking accuracy (ATE RMSE), while color smoothing enhances rendering quality (PSNR).

Sequences	Position	Only Color	Only	Depth L1	ATE RMSE	PSNR
				[cm] ↓	[cm] ↓	[dB] ↑
fr1/desk	X	X		2.93	3.36	21.85
	X	✓		2.59	2.65	23.52
	✓	X		2.30	2.28	22.61
	✓	✓		2.03	1.86	24.41
0169	X	X		6.55	12.13	18.79
	X	✓		6.20	11.03	19.86
	✓	X		5.91	10.12	19.23
	✓	✓		5.83	9.82	20.32

5 Conclusion

In this paper, we present a novel 3DGS-SLAM method that enhances robustness through an adaptive kernel smoothing strategy. We challenge the conventional wisdom that perfect visual fidelity is the primary determinant of tracking accuracy, demonstrating that a controlled rendering regularization effectively mitigates the impact of 3DGS parameter noise on pose tracking. Our core contribution is Corrective Blurry KNN (CB-KNN), a method that dynamically adjusts Gaussian parameters in local regions to produce a regularization effect during rendering, without altering the underlying map parameters. For computational efficiency, this strategy is applied only to keyframes. Experimental results demonstrate that our method significantly improves the accuracy and stability of pose tracking while maintaining high-quality map reconstruction.

References

1. Aliev, K.A., Sevastopolsky, A., Kolos, M., Ulyanov, D., Lempitsky, V.: Neural point-based graphics. In: European conference on computer vision. pp. 696–712. Springer (2020)
2. Bai, B., Qiao, X., Zhao, H.: Uncertainings: Uncertainty-aware indoor reconstruction via gaussian splatting. *Neurocomputing* p. 132136 (2025)
3. Bergmann, P., Wang, R., Cremers, D.: Online photometric calibration of auto exposure video for realtime visual odometry and slam. *IEEE Robotics and Automation Letters* **3**(2), 627–634 (2017)
4. Brateanu, A., Balmez, R., Avram, A., Orhei, C.: Akdt: Adaptive kernel dilation transformer for effective image denoising. *Proceedings Copyright* **418**(425), 19 (2025)
5. Buades, A., Coll, B., Morel, J.M.: A non-local algorithm for image denoising. In: 2005 IEEE computer society conference on computer vision and pattern recognition (CVPR’05). vol. 2, pp. 60–65. Ieee (2005)
6. Burri, M., Nikolic, J., Gohl, P., Schneider, T., Rehder, J., Omari, S., Achtelik, M.W., Siegwart, R.: The euroc micro aerial vehicle datasets. *The International Journal of Robotics Research* **35**(10), 1157–1163 (2016)
7. Campos, C., Elvira, R., Rodríguez, J.J.G., Montiel, J.M., Tardós, J.D.: Orb-slam3: An accurate open-source library for visual, visual-inertial, and multimap slam. *IEEE transactions on robotics* **37**(6), 1874–1890 (2021)
8. Cheng, L., Hu, J., Yan, H., Gladkova, M., Huang, T., Liu, Y.H., Cremers, D., Li, H.: Physically-based photometric bundle adjustment in non-lambertian environments. In: 2024 IEEE/RSJ International Conference on Intelligent Robots and Systems (IROS). pp. 10461–10468. IEEE (2024)
9. Dai, A., Chang, A.X., Savva, M., Halber, M., Funkhouser, T., Nießner, M.: Scannet: Richly-annotated 3d reconstructions of indoor scenes. In: *Proceedings of the IEEE conference on computer vision and pattern recognition*. pp. 5828–5839 (2017)
10. Engel, J., Koltun, V., Cremers, D.: Direct sparse odometry. *IEEE transactions on pattern analysis and machine intelligence* **40**(3), 611–625 (2017)
11. Engel, J., Schöps, T., Cremers, D.: Lsd-slam: Large-scale direct monocular slam. In: *European conference on computer vision*. pp. 834–849. Springer (2014)
12. Fleishman, S., Cohen-Or, D., Silva, C.T.: Robust moving least-squares fitting with sharp features. *ACM transactions on graphics (TOG)* **24**(3), 544–552 (2005)
13. Gao, K., Gao, Y., He, H., Lu, D., Xu, L., Li, J.: Nerf: Neural radiance field in 3d vision, a comprehensive review. *arXiv preprint arXiv:2210.00379* (2022)
14. Han, X., Liu, H., Ding, Y., Yang, L.: Ro-map: Real-time multi-object mapping with neural radiance fields. *IEEE Robotics and Automation Letters* **8**(9), 5950–5957 (2023)
15. Huang, B., Yu, Z., Chen, A., Geiger, A., Gao, S.: 2d gaussian splatting for geometrically accurate radiance fields. In: *ACM SIGGRAPH 2024 conference papers*. pp. 1–11 (2024)
16. Huang, H., Li, L., Cheng, H., Yeung, S.K.: Photo-slam: Real-time simultaneous localization and photorealistic mapping for monocular stereo and rgb-d cameras. In: *Proceedings of the IEEE/CVF Conference on Computer Vision and Pattern Recognition*. pp. 21584–21593 (2024)
17. Johari, M.M., Carta, C., Fleuret, F.: Eslam: Efficient dense slam system based on hybrid representation of signed distance fields. In: *Proceedings of the IEEE/CVF conference on computer vision and pattern recognition*. pp. 17408–17419 (2023)

18. Kang, W., Kim, J., Chung, J., Choi, S., Kim, T.w.: Efficient graduated non-convexity for pose graph optimization. In: 2024 24th International Conference on Control, Automation and Systems (ICCAS). pp. 545–548. IEEE (2024)
19. Keetha, N., Karhade, J., Jatavallabhula, K.M., Yang, G., Scherer, S., Ramanan, D., Luiten, J.: Splatam: Splat track & map 3d gaussians for dense rgb-d slam. In: Proceedings of the IEEE/CVF Conference on Computer Vision and Pattern Recognition. pp. 21357–21366 (2024)
20. Kerbl, B., Kopanas, G., Leimkühler, T., Drettakis, G.: 3d gaussian splatting for real-time radiance field rendering. *ACM Trans. Graph.* **42**(4), 139–1 (2023)
21. Li, B., Cai, Z., Li, Y.F., Reid, I., Rezatofighi, H.: Hier-slam: Scaling-up semantics in slam with a hierarchically categorical gaussian splatting. In: 2025 IEEE International Conference on Robotics and Automation (ICRA). pp. 9748–9754. IEEE (2025)
22. Liu, S., Deng, T., Zhou, H., Li, L., Wang, H., Wang, D., Li, M.: Mg-slam: Structure gaussian splatting slam with manhattan world hypothesis. *IEEE Transactions on Automation Science and Engineering* (2025)
23. Matsuki, H., Murai, R., Kelly, P.H., Davison, A.J.: Gaussian splatting slam. In: Proceedings of the IEEE/CVF Conference on Computer Vision and Pattern Recognition. pp. 18039–18048 (2024)
24. Peng, R., Xu, W., Tang, L., Liao, L., Jiao, J., Wang, R.: Structure consistent gaussian splatting with matching prior for few-shot novel view synthesis. *Advances in Neural Information Processing Systems* **37**, 97328–97352 (2024)
25. Sandström, E., Li, Y., Van Gool, L., Oswald, M.R.: Point-slam: Dense neural point cloud-based slam. In: Proceedings of the IEEE/CVF International Conference on Computer Vision. pp. 18433–18444 (2023)
26. Song, X., Zheng, J., Yuan, S., Gao, H.a., Zhao, J., He, X., Gu, W., Zhao, H.: Sags: Scale-adaptive gaussian splatting for training-free anti-aliasing. *arXiv preprint arXiv:2403.19615* (2024)
27. Straub, J., Whelan, T., Ma, L., Chen, Y., Wijnmans, E., Green, S., Engel, J.J., Mur-Artal, R., Ren, C., Verma, S., et al.: The replica dataset: A digital replica of indoor spaces. *arXiv preprint arXiv:1906.05797* (2019)
28. Sturm, J., Engelhard, N., Endres, F., Burgard, W., Cremers, D.: A benchmark for the evaluation of rgb-d slam systems. In: 2012 IEEE/RSJ international conference on intelligent robots and systems. pp. 573–580. IEEE (2012)
29. Sucar, E., Liu, S., Ortiz, J., Davison, A.J.: imap: Implicit mapping and positioning in real-time. In: Proceedings of the IEEE/CVF international conference on computer vision. pp. 6229–6238 (2021)
30. Wang, H., Wang, J., Agapito, L.: Co-slam: Joint coordinate and sparse parametric encodings for neural real-time slam. In: Proceedings of the IEEE/CVF Conference on Computer Vision and Pattern Recognition. pp. 13293–13302 (2023)
31. Wang, L., Chen, Y., Song, W., Xu, H.: Point cloud denoising and feature preservation: an adaptive kernel approach based on local density and global statistics. *Sensors* **24**(6), 1718 (2024)
32. Werner, T.: Applications of robust statistics in autonomous driving. *IEEE Access* (2025)
33. Werner, T.: Applications of robust statistics in autonomous driving. *IEEE Access* (2025)
34. Whelan, T., Leutenegger, S., Salas-Moreno, R.F., Glocker, B., Davison, A.J.: Elasticfusion: Dense slam without a pose graph. In: *Robotics: science and systems*. vol. 11. Rome (2015)

35. Woodford, O.J., Rosten, E.: Large scale photometric bundle adjustment. arXiv preprint arXiv:2008.11762 (2020)
36. Xin, Z., Wu, C., Huang, P., Zhang, Y., Mao, Y., Huang, G.: Large-scale gaussian splatting slam. In: 2025 IEEE International Conference on Robotics and Automation (ICRA). pp. 8478–8485. IEEE (2025)
37. Yan, C., Qu, D., Xu, D., Zhao, B., Wang, Z., Wang, D., Li, X.: Gs-slam: Dense visual slam with 3d gaussian splatting. In: Proceedings of the IEEE/CVF Conference on Computer Vision and Pattern Recognition. pp. 19595–19604 (2024)
38. Yan, Y., Lin, H., Zhou, C., Wang, W., Sun, H., Zhan, K., Lang, X., Zhou, X., Peng, S.: Street gaussians: Modeling dynamic urban scenes with gaussian splatting. In: European Conference on Computer Vision. pp. 156–173. Springer (2024)
39. Yang, X., Li, H., Zhai, H., Ming, Y., Liu, Y., Zhang, G.: Vox-fusion: Dense tracking and mapping with voxel-based neural implicit representation. In: 2022 IEEE International Symposium on Mixed and Augmented Reality (ISMAR). pp. 499–507. IEEE (2022)
40. Younes, M., Boukhayma, A.: Anti-aliased 2d gaussian splatting. In: The Thirty-ninth Annual Conference on Neural Information Processing Systems (2025)
41. Yu, A., Li, R., Tancik, M., Li, H., Ng, R., Kanazawa, A.: Plenotrees for real-time rendering of neural radiance fields. In: Proceedings of the IEEE/CVF international conference on computer vision. pp. 5752–5761 (2021)
42. Yu, Z., Chen, A., Huang, B., Sattler, T., Geiger, A.: Mip-splatting: Alias-free 3d gaussian splatting. In: Proceedings of the IEEE/CVF conference on computer vision and pattern recognition. pp. 19447–19456 (2024)
43. Yugay, V., Li, Y., Gevers, T., Oswald, M.R.: Gaussian-slam: Photo-realistic dense slam with gaussian splatting. arXiv preprint arXiv:2312.10070 (2023)
44. Zhang, J., Chen, K., Chen, S., Zheng, Y., Huang, T., Yu, Z.: Spikegs: 3d gaussian splatting from spike streams with high-speed camera motion. In: Proceedings of the 32nd ACM International Conference on Multimedia. pp. 9194–9203 (2024)
45. Zhou, L., Wang, S., Kaess, M.: π -lsam: Lidar smoothing and mapping with planes. In: 2021 IEEE international conference on robotics and automation (ICRA). pp. 5751–5757. IEEE (2021)
46. Zhu, Q., Wei, Z., Zheng, Z., Zhan, Y., Yao, Z., Zhang, J., Wu, K., Zheng, Y.: Rpbgs: Towards robust neural point-based graphics in the wild. In: European Conference on Computer Vision. pp. 389–406. Springer (2024)
47. Zhu, S., Qin, R., Wang, G., Liu, J., Wang, H.: Semgauss-slam: Dense semantic gaussian splatting slam. In: 2025 IEEE/RSJ International Conference on Intelligent Robots and Systems (IROS). pp. 21174–21181. IEEE (2025)
48. Zhu, Z., Peng, S., Larsson, V., Cui, Z., Oswald, M.R., Geiger, A., Pollefeys, M.: Nicer-slam: Neural implicit scene encoding for rgb slam. In: 2024 International Conference on 3D Vision (3DV). pp. 42–52. IEEE (2024)
49. Zhu, Z., Peng, S., Larsson, V., Xu, W., Bao, H., Cui, Z., Oswald, M.R., Pollefeys, M.: Nice-slam: Neural implicit scalable encoding for slam. In: Proceedings of the IEEE/CVF conference on computer vision and pattern recognition. pp. 12786–12796 (2022)